Conf-940843--18

GA–A21814

RECENT RESULTS FROM THE DIII–D TOKAMAK AND IMPLICATIONS FOR FUTURE DEVICES

by

J.L. LUXON for The DIII–D TEAM

FEBRUARY 1995

GENERAL ATOMICS

DISCLAIMER

DISCLAIMER

Portions of this document may be illegible in electronic image products. Images are produced from the best available original document.

GA–A21814

RECENT RESULTS FROM THE DIII–D TOKAMAK AND IMPLICATIONS FOR FUTURE DEVICES

by

J.L. LUXON for The DIII–D TEAM

This is a preprint of an invited paper presented at the 18th Symposium on Fusion Technology, August 22–26, 1994, in Karlsruhe, Germany, and to be printed in the *PROCEEDINGS*.

Work supported by
the U.S. Department of Energy
under Contract Nos. DE-AC03-89ER51114, W-7405-ENG-48,
DE-AC05-84OR21400, DE-AC03-76DP00769

GA PROJECT 3466
FEBRUARY 1995

TJ GENERAL ATOMICS

ABSTRACT

Improvements to the DIII–D tokamak have led to significant new research results and enhanced performance of the tokamak systems. These results provide important inputs to the design of next generation divertor systems including the upgrade of the DIII–D divertor.

Key results have been obtained in understanding of the divertor configuration and developing effective configurations for new devices. The use of graphite for the plasma facing components and careful wall preparation has enabled the routine achievement of regimes of enhanced energy confinement. In elongated discharges, triangularity has been found to be important in attaining good discharge performance as measured by the product of the normalized plasma pressure and the energy confinement time, $\beta\tau_E$. This constrains the design of the divertor configuration (X-point location). Active pumping of the divertor region using an in-situ toroidal cryogenic pump has demonstrated control of the plasma density in H–mode discharges and allowed the dependence of confinement on plasma density and current to be separately determined. Helium removal from the plasma edge sufficient to achieve effective ash removal in reactor discharges has also been demonstrated using this pumping configuration. The reduction of the heat flux to the divertor plates has been demonstrated using two different techniques to increase the radiation in the boundary regions of the plasma and thus reduce the heat flux to the divertor plates; deuterium gas injection has been used to create a strongly radiating localized zone near the X-point, and impurity (neon) injection to enhance the radiation from the plasma mantle.

Precise shaping of the plasma current profile has been found to be important in achieving enhanced tokamak performance. Transiently shaped current profiles have been used to demonstrate regimes of plasmas with high beta and good confinement. Control of

the current profile also is important to sustaining the plasma in the Very High (VH)–mode of energy confinement.

Ongoing and planned enhancements to the DIII–D tokamak systems will allow us to further exploit these gains. The recent upgrade of the ICRF system to 6 MW should allow sufficient current drive to begin independent control of the plasma current. Work is beginning on a radiative divertor modification to the vessel interior which will combine the desirable features of highly triangular plasma shape with strong pumping and baffling to minimize the back-streaming of gas and impurities.

CONTENTS

ABSTRACT iii

1. INTRODUCTION 1

Plasma Systems 5
Plasma Density and Particle Control 5
Divertor Power Flow and Erosion 10
Plasma Performance 15
Current Profile Control 22
Future Plans 22

REFERENCES 27

ACKNOWLEDGMENTS 29

APPENDIX I: DIII–D TEAM 31

LIST OF FIGURES

Fig. 1. The cross section of DIII–D with flux surfaces of a double-null divertor discharge superimposed 2

Fig. 2. The cross section of the divertor baffle and cryopump in the lower outer corner of the vessel 3

Fig. 3 Two examples from the experiment to determine the scaling of H–mode confinement with density and current 7

Fig. 4. Comparison of the evolution of the helium density near the plasma center measured with charge exchange recombination spectroscopy during discharges with and without Ar frost applied to the divertor cryopump 8

Fig. 5 Isometric view of the C-Coil 9

Fig. 6. Vacuum vessel cross section with magentic flux surfaces and zones of high radiated power from 48 channel bolometer array superimposed for discharge with no gas puff 11

LIST OF FIGURES (Continued)

Fig. 7. Vacuum vessel cross section with magentic flux surfaces and zones of high radiated power superimposed for a discharge with deuterium gas puffing at the edge 12

Fig. 8. Vacuum vessel cross section with magentic flux surfaces and zones of high radiated power superimposed for a discharge with neon injection 13

Fig. 9. A photograph of a DiMES sample inserted into the DIII–D divertor floor 14

Fig. 10. A comparison of results of the UEDGE model for the DIII–D divertor target heat flux with data from the IR camera 16

Fig. 11. Summary of the results achieved in plasma shape studies 17

Fig. 12. Rotational stabilization of the resistive wall mode allows high β values to be achieved 19

Fig. 13. Comparison of E_r, $E_r \times$ B shear, and Z_{eff} with and without magnetic braking of VH–mode plasmas 21

Fig. 14. Discharge prepared with fast negative current ramp and FW and EDCH power applied 23

Fig. 15. Cross section of the radiative divertor configuration being developed for DIII–D which will allow either single-, or double-null divertor operation 24

LIST OF TABLES

Table 1. Summary of characteristic parameters for the DIII–D tokamak 2

Table 2. The highest achieved plasma parameters for DIII–D 2

1. INTRODUCTION

The DIII–D tokamak has produced key results on stability, confinement, and understanding of the divertor along with demonstrations of fast wave current drive and heating. A combination of excellent device flexibility and timely hardware changes has led to significant inputs to the design of ITER, TPX, and other future devices. The DIII–D program focuses on achieving an effective divertor configuration for next generation tokamaks, while improving the tokamak configuration to achieve optimum performance for future reactor devices. Previous H–mode energy confinement scaling has been clarified and shown to depend linearly on the plasma current and be essentially independent of density. Effective helium ash removal, critical to the development of a reactor device, has been demonstrated. The role of the plasma shape in determining the overall performance has been further developed. The addition of new diagnostics has allowed substantially improved understanding of mechanisms for dissipating the power flowing to the plasma edge by radiation before it reaches the divertor target plates.

A strong collaborative effort has long been an important asset to the DIII–D program. The DIII–D program currently enjoys the active participation of seven U.S. National Laboratories, twelve international laboratories, and 15 universities. A vigorous interactive relationship is maintained with ITER and the U.S. TPX program.

The DIII–D tokamak is a 2.5:1 aspect ratio device capable of achieving a wide range of plasma cross sections (Fig. 1) [1]. The tokamak is normally operated with deuterium. The device parameters are summarized in Table 1. Improvements in the hardware and understanding of the tokamak performance have led to improvements in the achieved tokamak parameters (Table 2). Confinement regimes of 3.6 times L–mode, regimes of

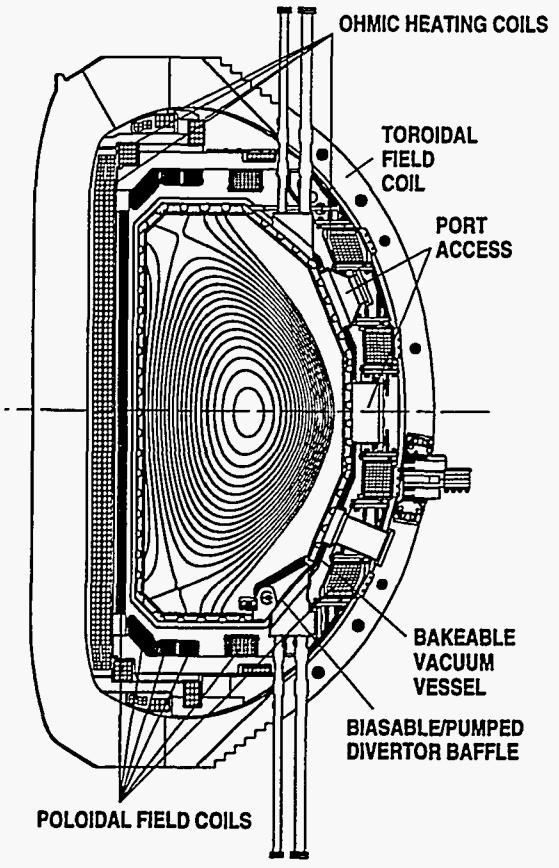

Fig. 1. The cross section of DIII-D with flux surfaces of a double-null divertor discharge superimposed.

Table 1
Summary of Characteristics Parameters for the DIII-D Tokamak

	PRESENT	PROPOSED
Major radius	1.67 m	
Minor radius	0.67 m	
Maximum toroidal field	2.2 T	
Available OH flux	10.5 V-sec	
Maximum plasma current*	3.0 MA	3.5 MA
Neutral beam power (80 keV)	20 MW	
RF power (110 GHz)	0.5 MW	4 →10 MW
RF power (30–120 MHz)	6 MW	8 MW
Current flattop (divertor at 2 MA)	5 sec	10 sec

*Divertor operation; Limiter operation of 3 MA achieved.

Table 2.
The Highest Achieved Plasma Parameters for DIII-D (not achieved simultaneously)

Average plasma toroidal beta, $\langle\beta_T\rangle$	12%
Central electron temperature, $T_e(0)$	7 keV
Central ion temperature, $T_i(0)$	21 keV
Line average electron density, $\bar{n}_e$	1.4×10^{20} m^{-3}
Total plasma energy, W	3.7 MJ
Plasma energy confinement time, τ_E	0.4 s (with 4 MW)
Confinement product, $n_e(0)\tau_E$	0.39×10^{20} m^{-3} s
Thermonuclear triple product, $n_D(0)T_i(0)\tau_E$	5×10^{20} m^{-3} keV s
H–mode duration	10.3 s

stable confinement with $\beta = 12.5\%$ and $\beta_N = 6$, and combined performance of $n_D(0)\tau_E T_i(0) = 5 \times 10^{20}$ m^{-3}-s-keV, [where $n_D(0)$ is the central deuterium density, τ_E is the energy confinement time, and $T_i(0)$ is the central ion temperature] have been demonstrated separately.

A number of recent improvements to the hardware systems have contributed significantly to results reported here. The interior of the tokamak chamber was covered completely with graphite tiles both to reduce the influx of metallic impurities and to provide protection of the Inconel vessel wall. A pumped divertor in the outer bottom portion of the chamber (Fig. 2) provides a means of particle control. A number of new diagnostics have been added with the particular focus of better understanding the characteristics of the divertor plasma and the plasma power balance. A motional Stark effect diagnostic is used in conjunction with the equilibrium analysis to better define the current profile and central q value.

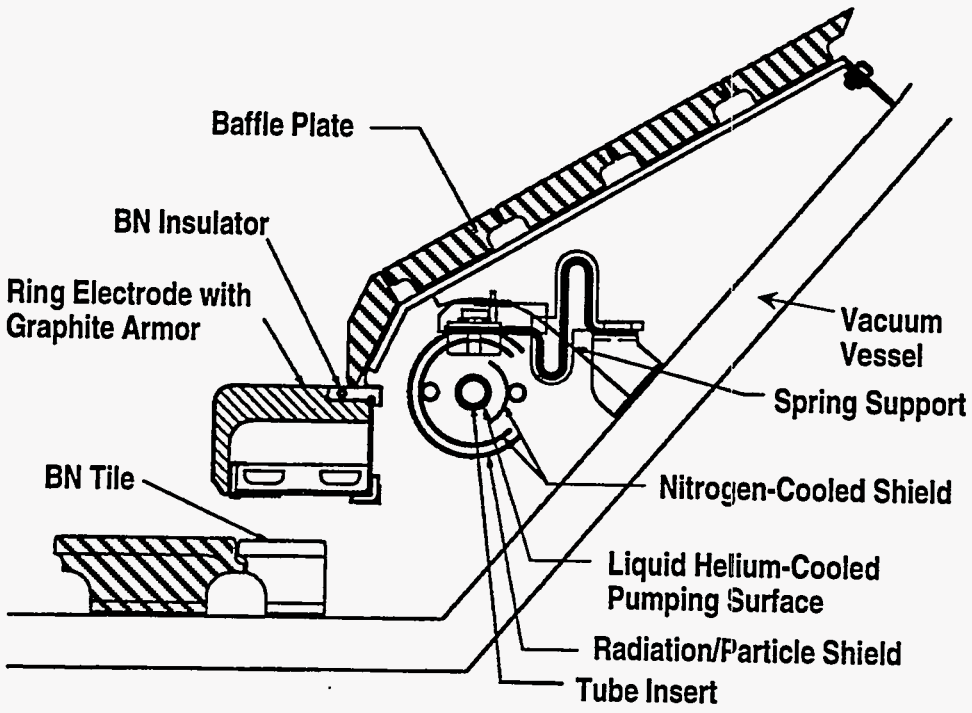

Fig. 2. Cross section of the divertor baffle and cryopump in the lower outer corner of the vessel.

Key to the achievement of many of the successes of DIII–D, has been the evolution of the plasma control system. Most recently, the use of digital techniques to control the plasma parameters has been added [2]. This system has substantially increased our flexibility in maintaining a wide variety of plasma shapes, and ability to control additional plasma parameters. Control of the plasma density during H–mode discharges has been achieved by varying the position of the outer divertor strike point of the discharge with respect to the pump aperture to control the pumping speed. Control of the ICRF antenna loading by the plasma, (by controlling the plasma antenna gap) the total plasma energy (by controlling the average neutral beam power), and a number of other quantities has also been implemented.

The present system utilizes relatively simple control algorithms which assume the control elements are essentially independent of each other. We will next install a system that uses a matrix characterization of the control system and advanced control techniques to achieve an even higher level of performance.

Substantial upgrades have also been made to the computing capabilities available to DIII–D. The need for these systems has been driven by a number of factors, including an increase in the size of the data set for each discharge (to 109 Mbytes recently), the increasing sophistication of hardware and diagnostics, an increasing amount of between-discharge and post-discharge analysis, and an increasing number of users, especially collaborators. The control and data acquisition computers are being replaced by UNIX based real time computer systems. Each computer system is now allowed to generate its own shot file, rather than accumulating all data into a single shot file. This allows data which has been collected by an individual diagnostic to be immediately accessible at both local and collaborator sites over the network. As a result of these changes, the time to acquire data between discharges has been reduced from 8.0 to 3.5 minutes.

Plasma Systems

Control of plasma impurities has proven crucial to the achievement of modes of good plasma confinement particularly in DIII–D. Several recent steps have been taken to dramatically reduce plasma impurities. The coverage of the Inconel walls with graphite was increased from 40% to essentially 100% (all of the walls except port apertures). The previously installed graphite tiles were temporarily removed from the walls and grit blasted with B_4C to remove surface impurities. All tiles were outgassed at 1000°C in vacuum [3,4]. The copper foam compliant material under the tiles was replaced with a graphite material eliminating a troublesome source of copper bursts in discharges. After completion of the installation and the usual 350°C bake, glow discharge wall conditioning was carried out with helium alone to avoid the formation of soot associated with hydrogen or deuterium discharge cleaning.

These steps resulted in dramatic decreases in plasma impurity levels and a remarkable improvement in plasma performance. Metallic impurities were substantially reduced, oxygen levels were reduced by a factor of 3 to 5, recycling levels were low and carbon impurities were not a problem. Operation with both H–mode and VH–mode regimes of enhanced energy confinement, successively more demanding indicators of a clean machine, was obtained early in the operating period, and ohmic H–mode discharges were obtained at full toroidal field for the first time. VH–mode discharges have since been used to obtain the highest values of the triple product yet attained in DIII–D.

Plasma Density and Particle Control

Control of the plasma density is important to the DIII–D program to allow discharges with H–mode confinement to be operated without the heretofore observed close dependence of the density on the plasma current. It is particularly important to demonstrate that H–mode confinement can be maintained at the lower densities favored for noninductive current drive. Demonstration of helium ash removal is essential to

developing a reactor. Without helium removal, the accumulation of helium in the core of the plasma will impede the D-T reactions and the burn will be terminated. In this section, the use of an in-situ divertor cryopump to achieve control of the discharge density and demonstrate helium removal will be described along with the development of a coil system to reduce the magnetic field asymmetries to make low density operation more accessible and the addition of a pellet injector to allow modification of the density profile.

The divertor cryopump consists of a toroidally continuous structure mounted beneath the divertor baffle plate at the bottom of the tokamak [5,6]. The liquid helium cooled inner tube is surrounded by a nitrogen shield and outer radiation shield (Fig. 2). The inner tube is electrically continuous allowing currents to flow during plasma initiation and disruptions. Disruption forces and thermal contraction/expansion during operation and the 350°C bake cycle are handled as hoop forces. The helium channel is carefully baffled to simultaneously achieve the helium flow rate and velocity necessary for stable operation. The particle exhaust rate from the plasma chamber depends on the location of the divertor strike point with respect to the pumping aperture. Pumping rates of as high as 200 Torr-l/s have been observed, but the rate is more typically a few tens of Torr-l/s [7].

The cryopump allows precise control of the plasma density by controlling the position of the outer divertor strike point with respect to the position of the pumping aperture. This is possible because of the highly localized distribution of neutral particles near the strike point. The plasma control system is used to vary the position of the strike point to maintain a preprogrammed density.

Control of the plasma density has allowed the functional dependence of H–mode confinement on plasma current and density to be determined [8]. This understanding is critical in applying otherwise well-characterized scaling relations [9] to the design of new devices. Heretofore, on DIII–D (and other tokamaks in general) the steady-state H–mode plasma density has been closely determined by the plasma current. In order to separate

the current and density dependence, deuterium single-null H–mode discharges were established with toroidal field $B_T = 2$ T and elongation $\kappa = 1.8$, and neutral beam power of $P_{NB} = 6$ MW was applied (Fig. 3). The cryopump was used to control the plasma density. Plasma currents of 0.75 MA and 1.5 MA were obtained at a density of 4×10^{19} m^{-3}. Similarly, discharges were run with a plasma current of 1.5 MA and densities of 4×10^{19} m^{-3} and 8×10^{19} m^{-3}. The other parameters identified in typical scaling laws (P_{NB}, R, a, B_T, κ) were held constant. The dependence of the confinement achieved on plasma current and density can be described by the power law relationship $\tau_E = 0.13 I_p^{0.94\pm0.06} n_e^{0.13\pm0.06}$, indicating that H–mode confinement is essentially linearly dependent on plasma current and independent of density.

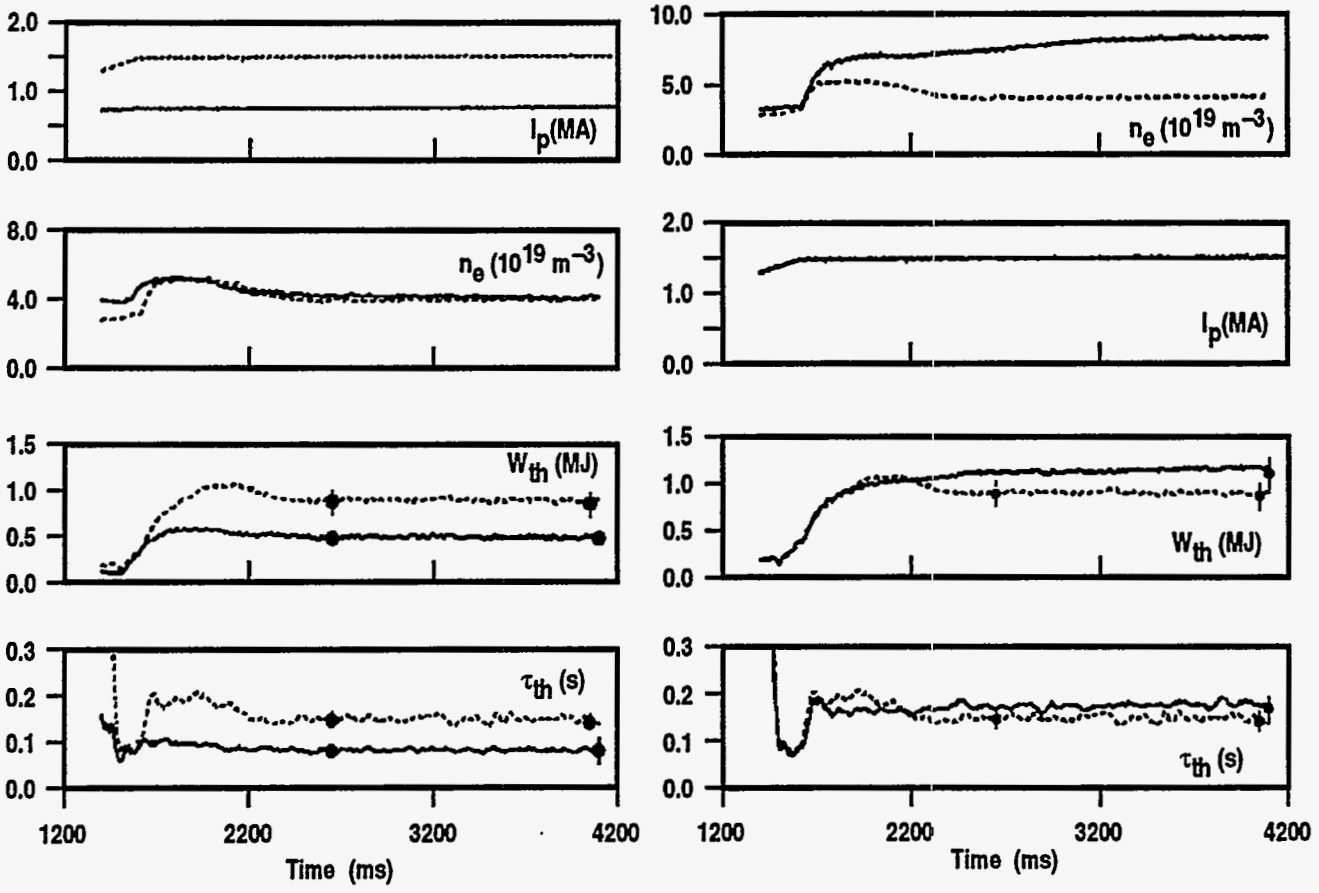

Fig. 3. Two examples from the experiment to determine the scaling of H-mode confinement with density and current. (a) Partial time history of two discharges with the densities held equal and different plasma currents. (b) Partial time histories of two discharges with the same plasma current and different densities.

Demonstration of the removal of helium ash from the core of the tokamak discharge is key to developing a reactor. Without helium removal, the accumulation of helium in the core of the plasma will impede the D-T reactions and the self-sustained burn will be lost. Using argon frost cryopumping techniques with the in-situ cryo-pump, pumping of helium in the vessel has been achieved [10]. Without pumping, when a short burst of helium was puffed into the edge of quasi steady-state discharges, the helium distribution would rapidly reach an equilibrium state indicating a recycling rate of near unity (Fig. 4). To achieve pumping, the outer strike point was moved near the divertor throat after the helium pulse. The gas still penetrated the discharge but was pumped away with a

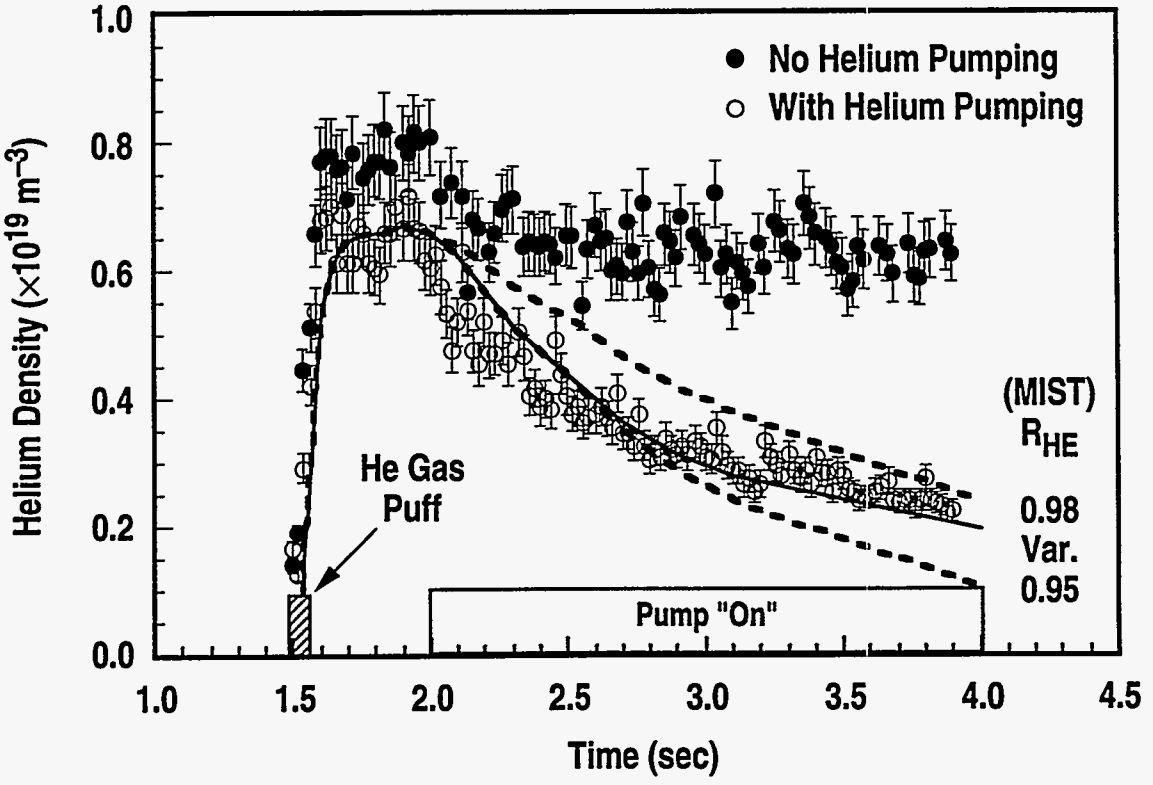

Fig. 4. Comparison of the evolution of the helium density near the plasma center measured with charge exchange recombination spectroscopy during discharges with and without Ar frost applied to the divertor cryopump. The dashed curves represent MIST transport calculations using different recycling models: constant R_{He} = 0.98 (upper dashed curve); steadily increasing R_{He} with R_{He} = 0.95 at the beginning (solid curve); and constant R_{He} = 0.95 (lower dashed curve). R_{He} is assumed to be unity before the OSP.

characteristic time of $\tau^*_{He} \sim 1.1$ s. Analysis indicates that $\tau^*_{He}/\tau_E = 8$. This result demonstrates that effective helium removal, within the range $\tau^*_{He}/\tau_E = 7–15$ identified as acceptable in recent reactor studies [11] can be achieved.

Operation at low plasma densities is especially useful for applying noninductive current drive techniques. However, low density operation is limited by locked modes caused by rotating modes locking onto magnetic field asymmetries intrinsic to the device field configuration [12]. In order to reduce the asymmetric component of the magnetic field in DIII–D, a new coil system which has the capability of adding an additional perturbation to the field with n=1, 2 or 3 is being installed (Fig. 5), with the principle purpose of canceling the existing field asymmetries to lower the minimum achievable plasma density. The coil system consists of six essentially equal picture frame coils mounted at the midplane external to the toroidal field coil and powered in diametrically opposite pairs. (The installation of this coil system on an operating tokamak posed considerable engineering and technical challenge owing to the number of interferences with existing components.)

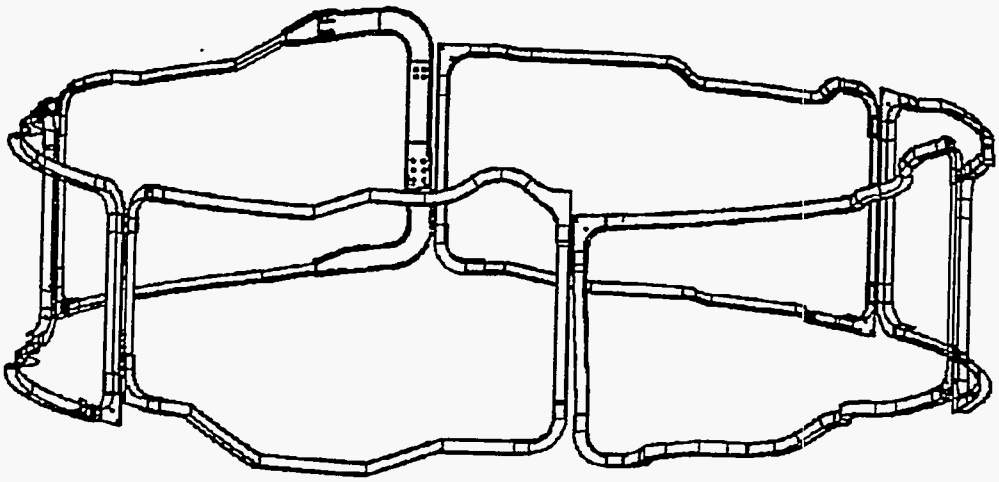

Fig. 5. Isometric view of the C-coil. The coil is centered vertically at the midplane of the tokamak and is slightly larger than the B-coil.

To allow modification of the plasma density profile, a three barrel pneumatic pellet injector developed by ORNL has been added to DIII–D. The injector produces hydrogen or deuterium pellets with sizes of 1.8 mm, 2.7 mm, and 4.0 mm and a repetition rate of up to 10 s^{-1}. Pellets are injected very near the midplane of the machine at velocities of up to 1 km/s. Initial operation with relatively small 1.8 mm pellets has demonstrated the ability to broaden the density profile as expected.

Divertor Power Flow and Erosion

Management and reduction of the energy flux to the divertor target plate is a key issue in divertor design, because the high flux of energetic particles can potentially cause severe erosion of the target material, and because high target temperatures can both lead to enhanced erosion and result in loss of structural integrity. The heat transported from the core to the boundary flows along a relatively narrow plasma channel to the divertor target plates. In present pulsed high heat flux machines such as DIII–D and JET, the divertor peak heat load reaches as high as 10 MW/m^2, which poses a challenging heat transfer problem. In future long pulse devices, the problem is exacerbated by the requirement of active cooling of the target plates and rapid erosion of the target plate material due to a high flux of ions at energies ≥ several tens of eV. One technique for managing this heat flow is to cause it to be radiated either from the main plasma or along the divertor leg before it reaches the target.

Two methods of dissipating the power flow before it reaches the divertor target plate have been evaluated in DIII–D; the use of high deuterium density in the divertor region to enhance the radiation in that region, and the use of impurity radiation to radiate the power from the plasma mantle inside the last closed flux surface. In typical ELMing H–mode divertor discharges, most of the plasma energy reaches the divertor target plates where it is largely concentrated near the outer strike point (Fig. 6). A zone of high

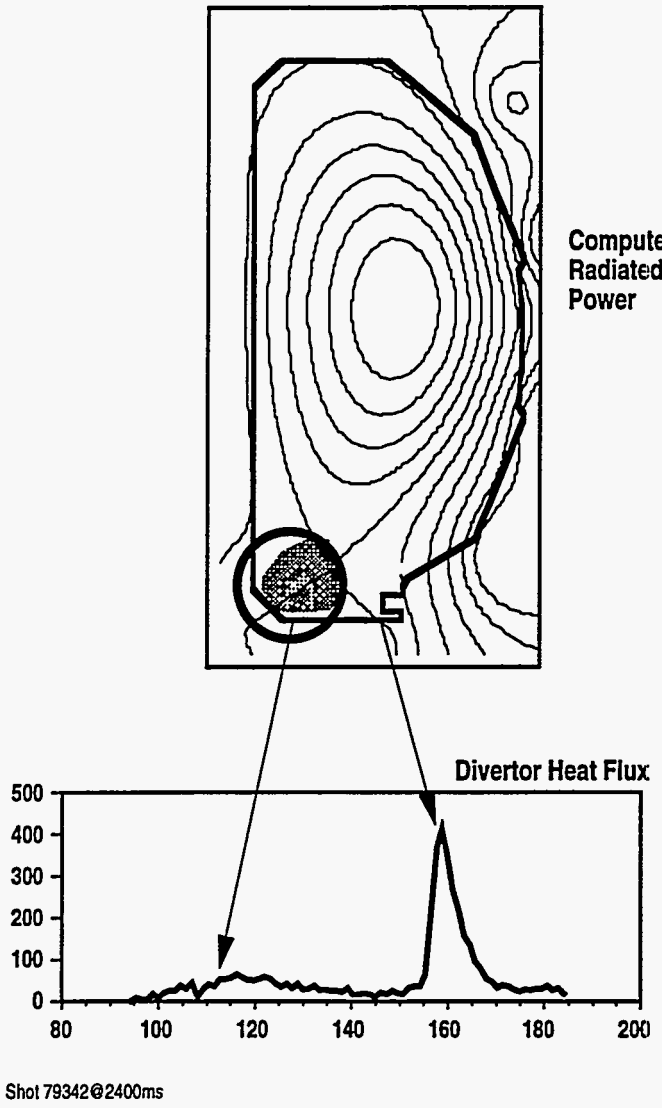

Fig. 6. (a) Vacuum vessel cross section with magnetic flux surfaces and zones of high radiated power from 48 channel bolometer array superimposed (in circle) for discharge with no gas puff. (b) The divertor target heat flux from the IR camera.

radiation along the inner leg of the divertor contributes to reducing the heat flux to the inner strike point. A deuterium gas flow of ~100 Torr-l/s into the plasma boundary region has been found to reduce the peak divertor heat flux by a factor of four (the location of the gas source has been found not to be important). These results are summarized in Fig. 7. The radiated power is computed from a 48 channel bolometer

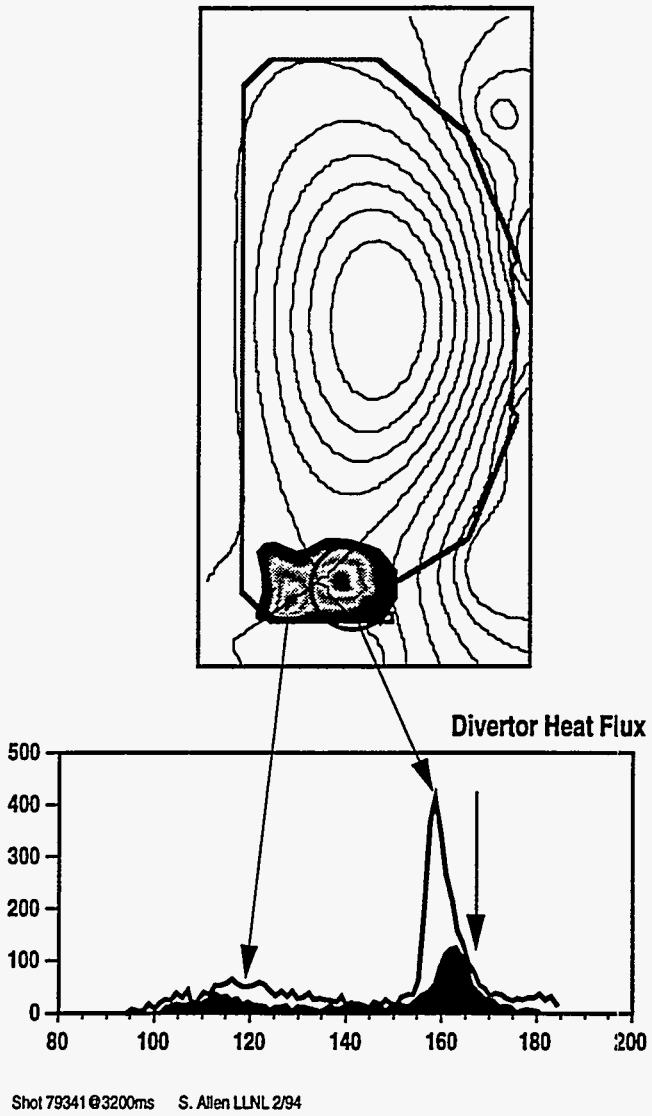

Fig. 7. (a) Vacuum vessel cross section with magnetic flux surfaces and zones of high radiated power superimposed for a discharge with deuterium gas puffing at the edge. (b) Divertor heat flux from the IR camera showing the reduced heat flux associated with the increased radiation at the outer outer divertor leg.

array. A region of strongly localized radiation is found both in the region of the divertor X-point and just outside the outer strike point. The gas flow results in an increase in the plasma density in these unpumped discharges and no more than a very small decrease in the energy confinement.

The injection of neon gas into the plasma edge reduces power reaching the divertor target by forming a thin radiating mantle near the core-plasma boundary (Fig. 8). This radiation is concentrated in the region just above the X-point, but a sizable part of it (50%) is spread throughout the entire mantle region. The resultant impurity content of the plasma is sufficient to increase the effective charge Z_{eff} of the plasma to about 3, and there is only a small decrease in confinement.

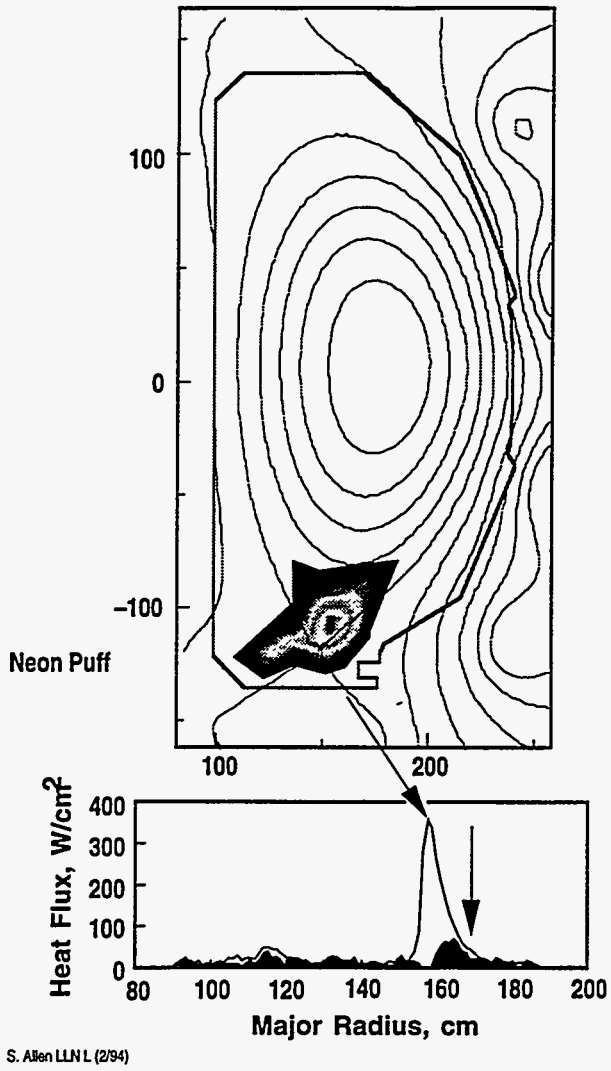

Fig. 8. (a) Vacuum vessel cross section with magnetic flux surfaces and zones of high radiated power superimposed for a discharge with neon injection. Not shown is the power radiated from the plasma edge. (b) The divertor target heat flux from the IR camera showing the reduction in heat flux associated with the impurity radiation.

It is critical to characterize and understand the interaction of the divertor plasma with the target and the erosion rate of divertor target materials for ITER and TPX. Models of the interaction of the energetic particle flux and wall are just reaching the point where meaningful comparisons to experiments can be made, and comprehensive diagnostic measurements of the characteristics of the incident flux are only now becoming available. Measurements have been made of plasma erosion in the DIII-D divertor target region using the DiMES diagnostic to insert samples into the divertor floor (Fig. 9). DiMES allows a 5 cm sample of material to be routinely inserted into the vessel floor and then removed in a total cycle time of as little as a few hours. A sample was exposed to 15 ELMing H-mode discharges. The average incident power on the samples was estimated to be roughly 0.5 MW/m^2. The erosion rate deduced from the measured net erosion was 60 nm and the maximum net erosion rate was 4 nm/s. The predicted erosion rate was

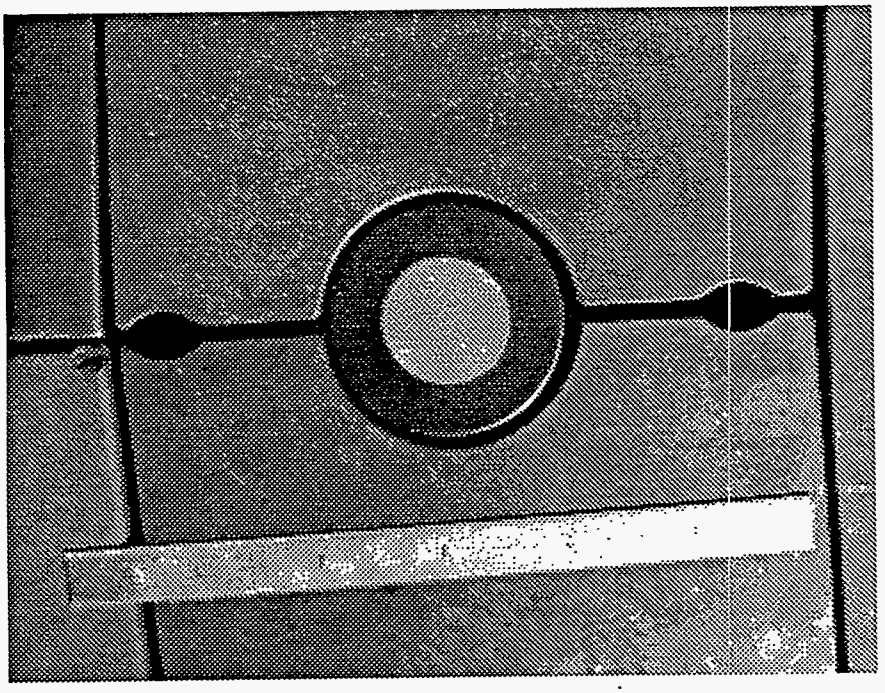

Fig. 9. A photograph of a DIMES sample inserted into the DIII-D divertor floor. This sample has a silicon wafer attached and is designed to help characterize the boronization films used to condition the DIII-D walls.

estimated using the limited experimental measurements of the edge plasma parameters available and edge boundary model codes [13]. The measured data is a factor of three greater than the model predictions where redeposition is included, but a factor of three less than is predicted with no redeposition. This result indicates that the high erosion rates predicted for graphite are essentially correct and redeposition is important, but the edge plasma data presently available does not allow precise comparison. Work is ongoing to improve these measurements.

In a second experiment, a 100 nm thick 1 cm diameter tungsten coating was applied to a graphite sample [14]. This sample was exposed to six ELM-free H–mode discharges with an average thermal flux of about 0.45 MW/m^2. The total net tungsten erosion was sufficiently small that it had to be estimated from the redeposition in the region around the sample, and was 0.8 nm, or 2.5 monolayers. This erosion is roughly 30 times less than would be expected with graphite and confirms the expectation that the heavier metals are much less susceptible to erosion than graphite.

Extensive models are being developed for the edge plasma and plasma wall interaction. These models are needed both to understand the results of present day experiments and to extrapolate them to future machines [15]. New diagnostic activities have also strongly focused on providing improved measurements of the edge plasma and divertor regions. Modeling of the edge plasma is done using the 2–D fluid model code UEDGE. An example of the modeling of the heat flux to the divertor is shown in Fig. 10. This code is used to provide input to DEGAS, a Monte Carlo neutral transport model, and MCI, a 3–D Monte Carlo impurity model, which is in development. Impurity transport is also modeled using MIST as was illustrated in Fig. 4 and NEWT-1D.

Plasma Performance

Understanding the role of plasma shape in achieving good overall plasma performance is an important issue for next generation devices. An experiment was

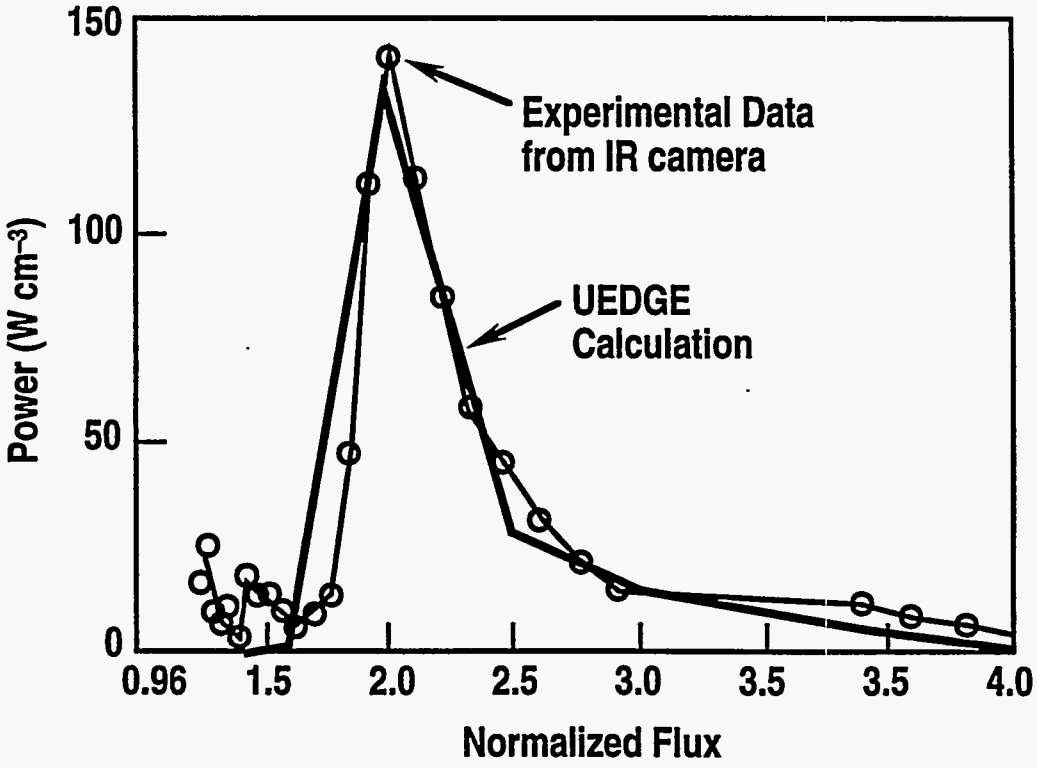

Fig. 10. A comparison of results of the UEDGE model for the DIII-D divertor target heat flux with data from the IR camera. A relative shift of normalized flux = 0.01 has been introduced to align the data with the theory.

carried out in which both the elongation and triangularity of double-null discharges were varied to separate the roles of these two parameters in determining the discharge performance as measured by $\beta\tau_E$ [16]. This result is crucial to the design of more specialized divertor configurations where precise control of the divertor channel geometry requires that the plasma configuration remain relatively fixed throughout a substantial part of the life of the experiment. It is immediately important in determining the shape of the plasma cross section to be used in the upgrade of DIII-D currently being designed. The result has also influenced the choice of cross-section for TPX. The experiment was carried out in double-null divertor plasmas with a toroidal field of 2 T. The cross-sections of the discharges studied are shown in Fig 11. For each cross-section, the plasma current was adjusted to achieve values of $q_{95} = 3.3$, 4.2, and 5.1. The density

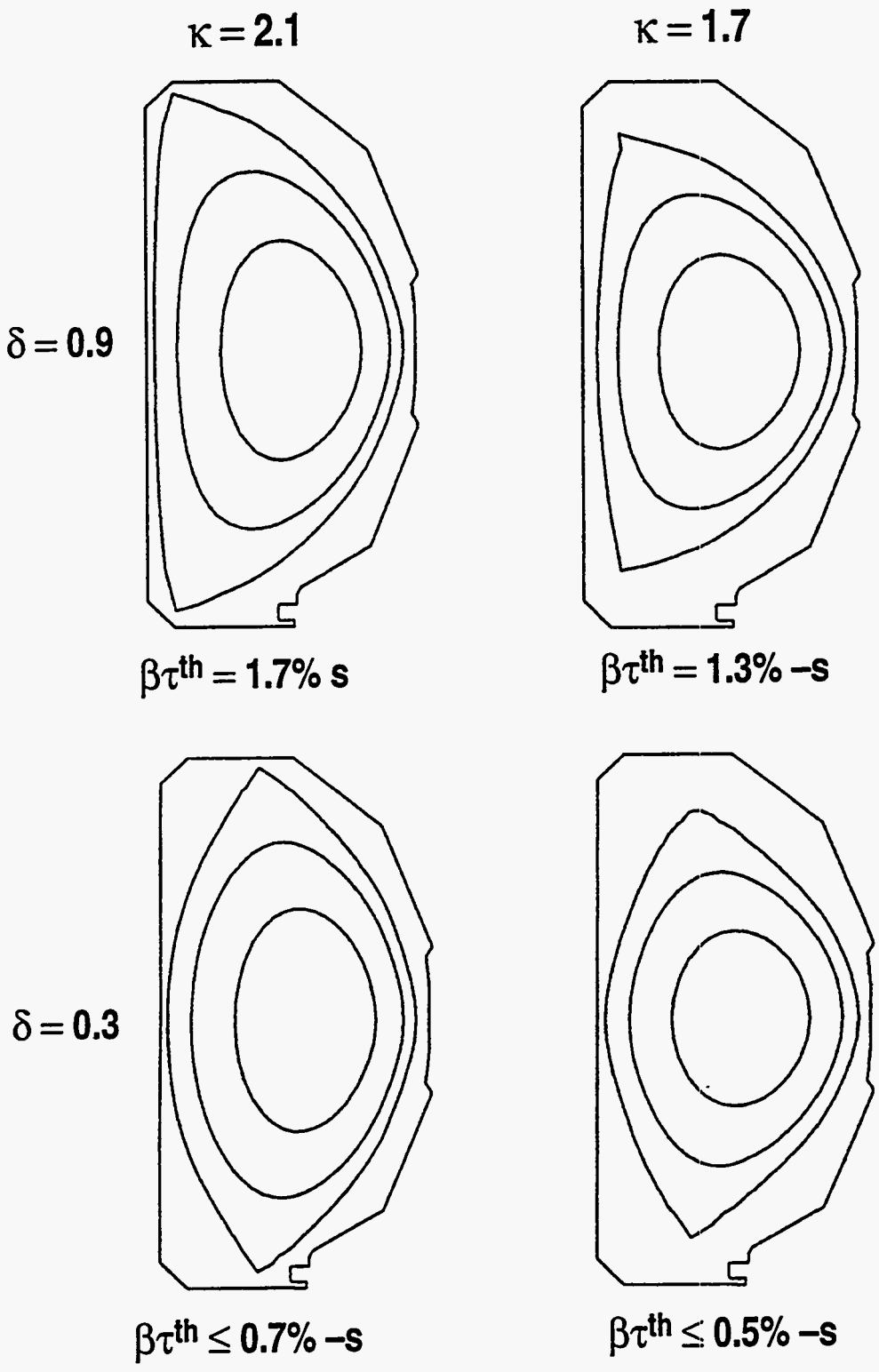

Fig. 11. Summary of the results achieved in plasma shape studies.

varied with plasma current as is typical in unpumped H–mode discharges. The neutral beam power was then increased to determine the maximal value of $\beta\tau_E$ that could be achieved in the discharge. The best result for each plasma shape is summarized in Fig. 11. The principle result is that the triangularity and elongation are both important in determining the overall performance of the discharge. It is also found that whether the discharge is single-null or double-null has not possible to form a high triangularity discharge without forming an essentially double-null shape).

Understanding the limits on plasma beta is also critical to the design of next generation tokamaks. Experiments at DIII–D have demonstrated high values of β = 12.5% and β_N = 6, and developed considerable understanding of the underlying theory [17,18]. Recent high β discharges in DIII–D have provided convincing evidence that a resistive wall can stabilize the ideal n = 1 kink mode for times much longer than the resistive wall penetration time. Beta values were achieved which were near those expected with a perfectly conducting wall at the location of the DIII–D vacuum vessel and up to 40 percent above the theoretically expected limit for no wall stabilization. The discharges were operated in a full-sized double null divertor configuration with low internal inductance, obtained by a slow positive current ramp and early beam heating, so as to maximize the coupling to the vacuum vessel wall and the possible gain in β. The discharge described in Fig. 12 was subject to detailed analysis. In this discharge, β_N was ramped up to β_N = 3.8 (β = 6%) using 18 MW of co-injected neutral beam heating, and q_o was maintained above 1.0. The expected β limit with no wall was β_N = 2.8. The period of high β was maintained for more than ten resistive wall relaxation times and ended only when the plasma rotation slowed.

Ideal stability analyses, coupled with accurate equilibrium reconstructions, show that the discharge is expected to be stable with a perfectly conducing wall at the location of the resistive DIII–D vacuum vessel, but ideally unstable if there is no wall. This result is

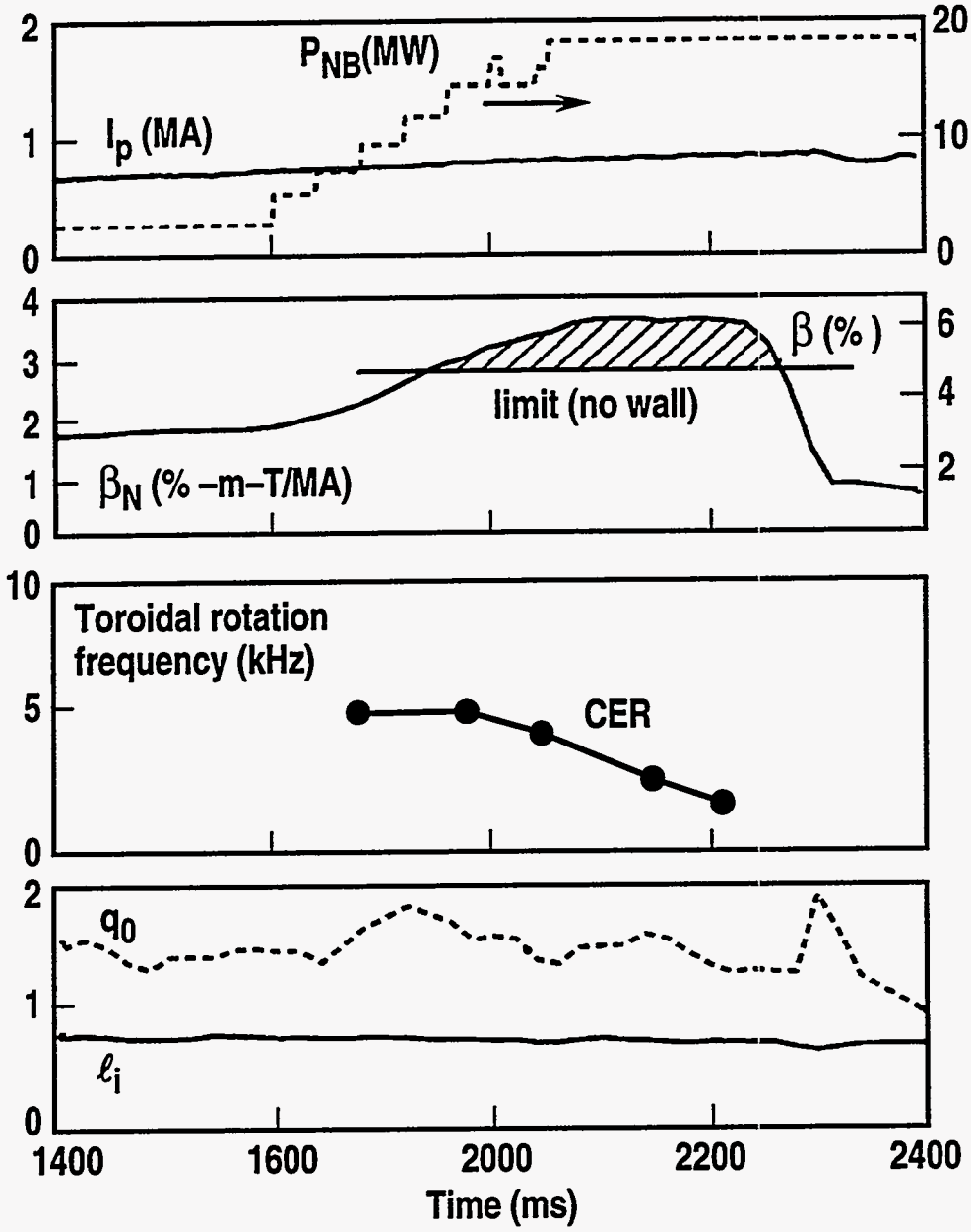

Fig. 12. Rotational stabilization of the resistive wall mode allows high β values to be achieved.

confirmed by detailed sensitivity studies with respect to variables in the equilibrium reconstructions and wall stabilization is found for several times with no sign of any of the slowly growing MHD modes that have been predicted [17,19] when the wall is resistive.

Plasma rotation is found to be essential for maintaining the enhanced wall stabilization. All the wall stabilized discharges were strongly neutral beam heated and were consequently rotating at a significant fraction (about 0.3) of the sound speed. However, in many discharges, the rotation slowed and slowly growing modes appeared with growth times close to the wall penetration time. These were locked from onset to the wall and bear all the hallmarks of the unstable resistive wall mode that is predicted by the early simple MHD theories. This mode then ultimately contributed to termination of the discharges. The cause of the slow-down in rotation, has not yet been clearly identified.

Stabilization of the resistive wall mode by plasma rotation has recently been predicted [18] by numerical calculations from coupling of the mode to strongly damped acoustic modes. When the rotation is much slower than the sound speed, however, the stabilization is lost, in agreement with the observations in the DIII–D wall stabilization experiments.

Energy confinement in tokamaks is characterized in terms of a number of different regimes (L–mode, H–mode, VH–mode, ...) often with sharp transitions during a discharge between one regime and another. The understanding of these regimes and the transition between them is still evolving. The confinement improvement in the plasma core seen following the transition from H–mode to VH–mode has been hypothesized to be due to a positive feedback mechanism occurring when the flow shear increases, say due to an increase in the plasma rotation, thereby decreasing turbulence and thus transport [20]. In recent DIII–D experiments the inverse process was demonstrated, a decrease in the $E \times B$ flow shear has been clearly related to the confinement decrease seen in plasma already in VH–mode confinement by using magnetic braking to slow the plasma rotation [21,22]. In the core, the shear flow is dominated by the radial electric field term E_r due primarily to the ion toroidal rotation. A non-axisymmetric perturbing (dipole) field centered above the toroidal field coil at R = 1.6 m was used to provide the braking and

lower the rotational velocity (magnetic braking) thus lowering the shear flow substantially [Fig.13(a,b)]. Turbulence increases and the transport increases to a considerably higher level. The single fluid diffusivity is seen to increase significantly, especially in the region where the change in shear flow is the greatest [Fig. 13(c)].

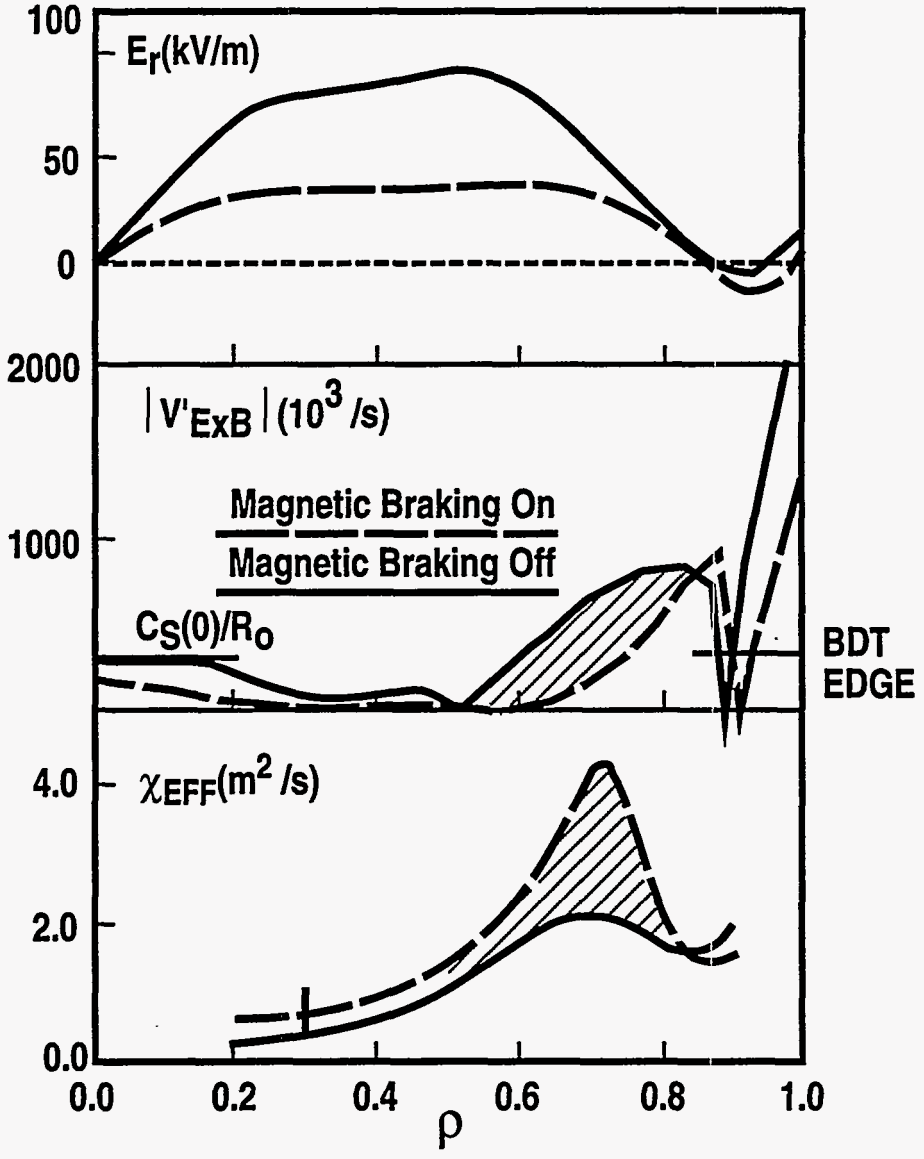

Fig 13. Comparison of E_r, $E_r \times B$ shear, and Z_{eff} with and without magnetic braking of VH-mode plasmas.

Current Profile Control

It is a goal of the DIII–D program to use non-inductive current drive to modify the plasma current profile in order to obtain improved plasma performance and to achieve total non-inductive plasma current. Fast waves have also been used to effectively heat the electrons independent of the toroidal field by setting the antenna phase to launch non-directional waves. Past experiments using transient inductive techniques have demonstrated that control of the plasma current profile is a path to improved plasma performance [23]. Recent experiments have also demonstrated total non-inductive current drive using fast waves in the ion cyclotron frequency range (FWCD) in plasmas heated with electron cyclotron resonance heating (ECRH) [24]. In this experiment, the plasma current was ramped down from 0.4 MA to 0.17 MA resulting in both improved energy confinement and RF absorption. During and following the rampdown, 0.8 MW of 60 GHz ECRH power was applied to heat the electrons and 1.5 MW of FW power was applied with the phase of the antenna adjusted to produce a unidirectional wave. Following the rampdown, the loop voltage remained negative until the end of the rf pulse, an interval of about three profile relaxation times, indicating that full noninductive current drive had been attained (Fig. 14). To confirm this result, the phasing of the FWCD antennas was adjusted to launch a symmetric wave while the phase velocity was maintained so that only heating of the electrons was expected; the voltage was positive at the end of the rf pulse. Presently, additional FW power systems are being commissioned to provide up to 6 MW of power, which is predicted to be adequate to produce fully noninductive discharges with current in the range 0.4 MA to 1.0 MA [25].

Future Plans

The DIII–D program will continue to focus on the understanding and development of both the divertor configuration and the advanced tokamak. The divertor element will

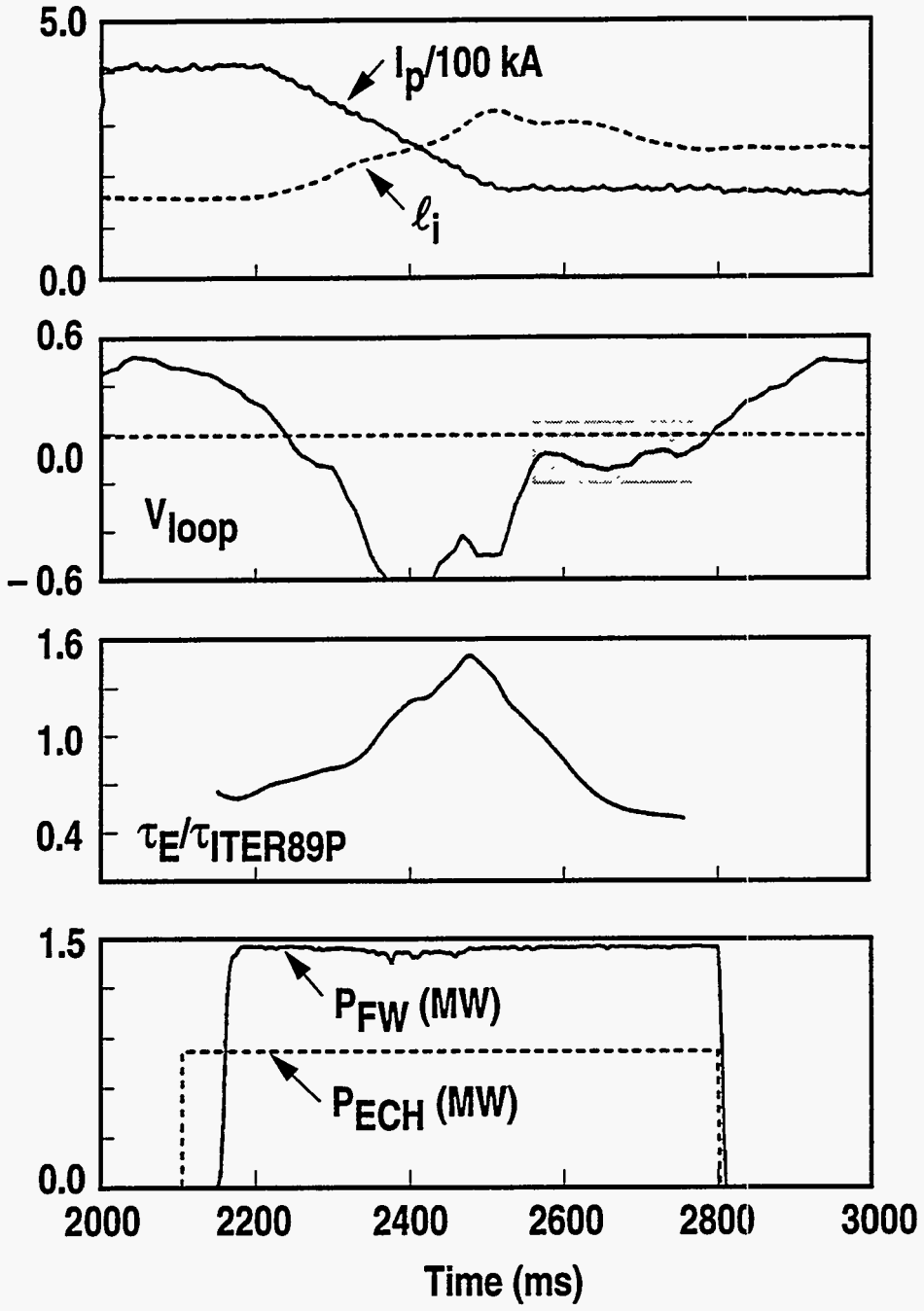

Fig. 14. Discharge prepared with fast negative current ramp and FW and ECH power applied. After the rampdown, the plasma current (0.17 MA) is sustained noninductively for the remainder of the RF pulse.

focus on the understanding of the present open divertor configuration which has a great deal of flexibility. New diagnostics are providing substantially improved characterization of the divertor region for comparison with developing models. In parallel, a new radiative divertor configuration is being designed for DIII–D (Fig. 15) [26]. The design

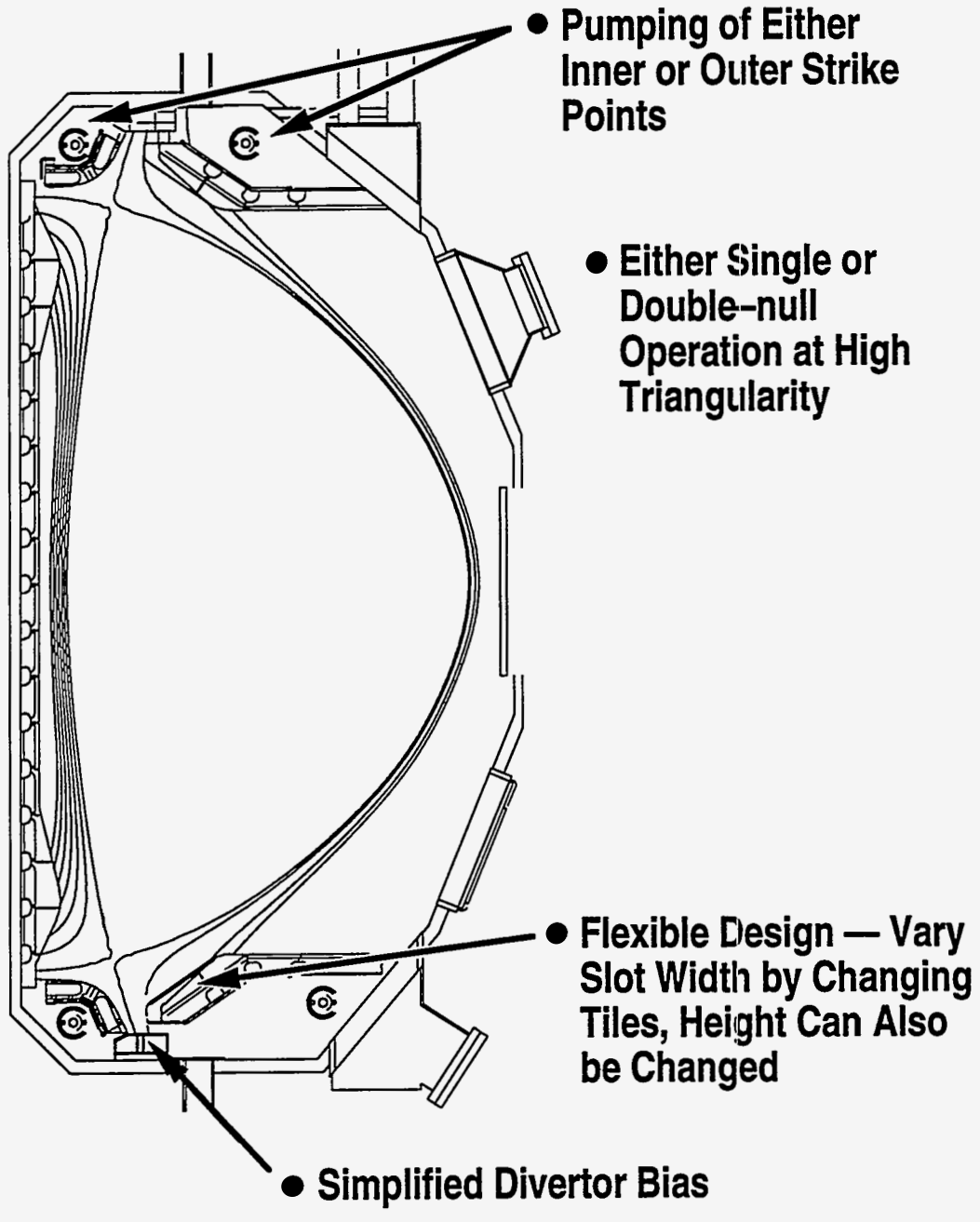

Fig. 15. Cross section of the radiative divertor configuration being developed for DIII-D which will allow either single-, or double-null divertor operation.

is based on many of the results discussed above. This modification will provide a more closed divertor configuration with higher triangularity [27]. Slot type divertor channels will be used to reduce the flow of neutrals back to the plasma, and radiation will be used to dissipate the heat flux before it reaches the divertor target. Extensive in-situ pumping will provide control of the neutral gas level. The design will also provide the capability for changing the slot length over a range of 23 cm to 43 cm. A few months of work in the vessel would be needed to make the change.

Key to the further development of advanced tokamak configurations with improved confinement and stability properties is the control of the current profile with quasi-steady state techniques. The DIII–D program is presently commissioning 4 MW of FWCD power which will raise our present capability to a total power of 6 MW. We plan to add 10 MW of ECH power at 110 GHz with 1 MW gyrotrons to provide off-axis current drive to augment bootstrap current and enhance the effectiveness of the on-axis FWCD. The availability of the radiative divertor configuration discussed above will then provide density control and elevated electron temperatures.

REFERENCES

[1] J.L. Luxon and L. Davis, Fusion Technol. **8** (1985) 441.

[2] J.R. Ferron and E.J. Strait, Rev. Sci. Instrum. **63** (1992) 4789.

[3] G.L. Jackson, et al., J. Nucl. Mater. **196–198** (1992) 236.

[4] K.L. Holtrop, et al., J. Vac. Sci. Technol. A **12** (1994) 1269

[5] J.P. Smith, et al., in Proc. 15th Symp. on Fusion Engineering, IEEE (Hyannis, Massachusetts, 1993) Vol. 2, p. 1043.

[6] K.M. Schaubel, et al., this conference.

[7] K.M. Schaubel, et al., Advances in Cryogenic Engineering **39** (1994).

[8] J.P. Christiansen, et al., Nucl. Fusion **32** (1992) 291.

[9] D.P. Schissel, et al., Nucl. Fusion to be published.

[10] M.R. Wade, et al., in Proc. 11th International Conference on Plasma Surface Interactions in Fusion Devices, (Ibarakaki-ken, Japan 1993) (to be published).

[11] D. Reiter, et al., Nucl. Fusion **30** (1990) 214.

[12] R.J. La Haye, et al., Phys. Fluids B **4** (1992) 2098.

[13] T.Q. Hua and J.N. Brooks, in Proc. 11th International Conference on Plasma Surface Interactions in Fusion Devices (Ibarakaki-ken, Japan 1993) (to be published).

[14] R. Bastasz, et al., in Proc. 11th International Conference on Plasma Surface Interactions in Fusion Devices (Ibarakaki-ken, Japan 1993) (to be published).

[15] M.E. Fenstermacher, et al., in Proc. 11th International Conference on Plasma Surface Interactions in Fusion Devices (Ibarakaki-ken, Japan 1993) (to be published).

[16] E.A. Lazarus, et al., Proc. 20st European Conference on Controlled Fusion and Plasma Heating, Lisbon, Portugal, 1993 (European Physical Society, Petit-Lancy, Switzerland, 1993) Vol. 17C, Part I, p. 95.

[17] J.P. Friedberg, *Ideal Magneto Hydrodynamics,* (Plenum Press, New York, 1987).

[18] L. Zakharov and S. V. Purvinskii, Sov. J. Plasma Phys. **13** (1987) 68 .

[19] A. Bondeson and D.J. Ward, Phys. Rev. Lett. **72** (1994) 2709.

[20] G.M. Staebler, et al. Phys. Plasmas **1** (1994) 909.

[21] K.H. Burrell, Phys Plasmas **1** (1994) 1536 .

[22] R.J. La Haye, et al., in *Local Transport Studies in Fusion Plasmas*, Proc. of the Varenna Workshop, 1993 (Societa Italiana di Fisica, Bologna, in press).

[23] T.S. Taylor, et al., in Proc. 21st European Conference on Controlled Fusion and Plasma Heating, Lisbon, Portugal, 1994 (European Physical Society, Petit-Lancy, Switzerland, to be published).

[24] R.I. Pinsker, R., et al., in Proc. 21st European Conference on Controlled Fusion and Plasma Heating, Lisbon, Portugal, 1994 (European Physical Society, Petit-Lancy, Switzerland, to be published).

[25] R.W. Callis, et al., this conference.

[26] S.L. Allen, et al., in Proc. 11th International Conference on Plasma Surface Interactions in Fusion Devices (Ibarakaki-ken, Japan 1993) (to be published).

[27] J.P. Smith, et al, this conference.

ACKNOWLEDGMENTS

Work supported by the U.S. Department of Energy under Contract Nos. DE-AC03-89ER51114, W-7405-ENG-48, DE-AC05-84OR21400, DE-FG03-89ER51121, DE-FG03-86ER53225, and DE-AC03-76DP00789. I would like to acknowledge the work of the entire DIII-D Team and the help of A.D. Turnbull and C.M. Greenfield in preparing this manuscript.

APPENDIX I: DIII-D TEAM

F. Allais,[a] S.L. Allen,[b] M.E. Austin,[c] D.R. Baker, C.B. Baxi, N.H. Brooks, D. Buchenauer,[d] K.H. Burrell, R.W. Callis, G.L. Campbell, T.N. Carlstrom, W.P. Cary, V.S. Chan, S.C. Chiu, M.S. Chu, S. Coda,[e] J.W. Cummings, J. Cuthbertson,[b] J.C. DeBoo, J.S. deGrassie, M. DiMartino, J.L. Doane, R.R. Dominguez, E.J. Doyle,[f] R.G. Evanko, T.E. Evans, J.R. Ferron, R.L. Freeman, D. Finkenthal,[g] C. Forest, P. Gohil, A.M. Gootgeld, K.L. Greene, C.M. Greenfield, R.J. Groebner, R.W. Harvey, W.W. Heidbrink,[h] P.A. Henline, D.N. Hill,[b] D.L. Hillis,[i] F.L. Hinton, T.R. Hodapp, K. Holtrop, J. Hogan, M.A. Hollerbach, R-M. Hong, C.L. Hsieh, D.A. Humphreys, A.W. Hyatt, H. Ikezi, G.L. Jackson, R.A. James,[b] T.H. Jensen, R. Jong,[b] K.M. Keith, A.G. Kellman, D.H. Kellman, R. Khayrutdinov,[j] J. Kim, Y. Kim,[k] N.P. Kirkpatrick, S. Konoshima,[l] R.J. La Haye, L.L. Lao, G.J. Laughon, E.A. Lazarus,[i] R. Lee, A.W. Leonard, J.A. Leuer, Y-R. Lin-Liu, S.I. Lippmann, J.M. Lohr, T.C. Luce, V. Lukash,[j] J.L. Luxon, M.A. Mahdavi, W.B. McHarg, E. McKee, M.M. Menon,[i] S.M. Miller, C.P. Moeller, R.A. Moyer,[f] A. Nerem, M.P. Nilsen, R. O'Neill, I. Opimach,[j] T.H. Osborne, D.O. Overskei, L. Owen,[i] W.A. Peebles,[f] P.I. Petersen, P.M. Petrach, T.W. Petrie, C.C. Petty, D.A. Phelps, R.D. Phelps, J. Phillips, R.I. Pinsker, P.A. Politzer, G.D. Porter,[b] R. Prater, E.E. Reis, D.B. Remsen, M.E. Rensink,[b] C.L. Rettig,[c] T. Rhodes,[f] J. Robinson, D. Rothweil, E. Ruskov,[h] M.J. Schaffer, K. Schaubel, D.P. Schissel, J.T. Scoville, R.P. Seraydarian, D.L. Sevier, T.C. Simonen, J.P. Smith, R.T. Snider, M. Srinivasan, G.M. Staebler, R.D. Stambaugh, H. St. John, R.E. Stockdale, E.J. Strait, P.L. Taylor, T.S. Taylor, D.M. Thomas, M.P. Thomas, S.J. Thompson, P.A. Thurgood V. Trukhin,[m] A.D. Turnbull, J. Vanderlann, M. Wade,[i] R.E. Waltz, J. Watkins,[n] W.P. West, J. Wight, C.P.C. Wong, R. Wood,[b] and D. Wroblewski[b]

PERMANENT ADDRESS

(a) University of Paris, France
(b) Lawrence Livermore National Laboratory, USA
(c) University of Maryland, USA
(d) Sandia National Laboratories, Livermore, USA
(e) Massachusetts Institute of Technology, USA
(f) University of California at Los Angeles, USA
(g) University of California at Berkeley, USA
(h) University of California at Irvine, USA
(i) Oak Ridge National Laboratory, USA
(j) Kurchatov Laboratory, Troitsk, Russia
(k) University of California at San Diego, USA
(l) Japan Atomic Energy Research Institute, Japan
(m) Kurchatov Institute, Moscow, Russia
(n) Sandia National Laboratories, Albuquerque, USA